THE JOURNAL OF PHYSICAL CHEMISTRY Letters

Letter

Cite This: J. Phys. Chem. Lett. 2019, 10, 6144−6150

pubs.acs.org/JPCL

Simultaneous Existence of Confined and Delocalized Vibrational Modes in Colloidal Quantum Dots

Albert Liu,[†] Diogo B. Almeida,[†] Wan-Ki Bae,[‡] Lazaro A. Padilha,[§] and Steven T. Cundiff*[,†]

[†]Department of Physics, University of Michigan, Ann Arbor, Michigan 48109, United States

[‡]SKKU Advanced Institute of Nano Technology, Sungkyunkwan University, Suwon, 16419 Gyeonggi, Republic of Korea

[§]Instituto de Fisica "Gleb Wataghin", Universidade de Campinas, Campinas, 13083-970 Sao Paulo, Brazil

Supporting Information

ABSTRACT: Coupling to phonon modes is a primary mechanism of excitonic dephasing and energy loss in semiconductors. However, low-energy phonons in colloidal quantum dots and their coupling to excitons are poorly understood because their experimental signatures are weak and usually obscured by the unavoidable inhomogeneous broadening of colloidal dot ensembles. We use multidimensional coherent spectroscopy at cryogenic temperatures to extract the homogeneous nonlinear optical response of excitons in a CdSe/CdZnS core/shell colloidal quantum dot ensemble. A comparison to the simulation provides evidence that the observed lineshapes arise from the coexistence of confined and delocalized vibrational modes, both of which couple strongly to excitons in CdSe/CdZnS colloidal quantum dots.

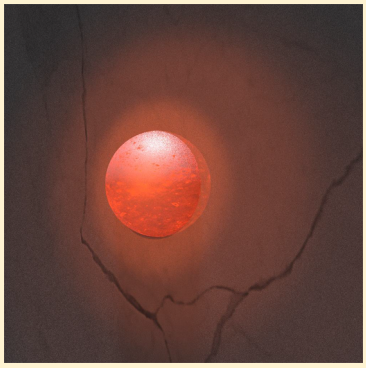

Semiconductor quantum dots, structures that confine electronic excitations in three dimensions, are a maturing technology that have potential applications in numerous areas of optoelectronics. These include areas such as single-photon emitters,[1,2] quantum computing,[3−5] and photovoltaics.[6,7]

Although the development of practical quantum dot devices is rapidly progressing, most areas of quantum dot optoelectronics suffer from the common issue of vibrational coupling to excitons.[8,9] Interactions between electronic excitations and lattice vibrations facilitate energy loss through nonradiative decay processes and play a vital role in coherent control protocols.[10−12] Acoustic vibrational modes are of particular importance because their low energies mediate coupling between the fine-structure of an exciton manifold[13−15] and comprise the primary dephasing mechanism of interband coherences[16−21] in quantum dots. Although usually a continuum of modes, acoustic vibrations can assume discrete modes[22,23] due to size confinement in colloidal quantum dots.[24−27] However, the two pictures of acoustic vibrations as a bulk-like phonon continuum or as discrete spherical harmonics are seldom simultaneously considered.

Vibrational coupling to excitons in quantum dots has been extensively studied, but most spectroscopic studies have utilized linear techniques such as absorption and photoluminescence. Linear spectrocopies encounter two main obstacles. First, ensembles of all types of quantum dots exhibit inhomogeneous broadening (due to dot size dispersion) of their absorption and emission profiles. Linear techniques only provide the inhomogeneous lineshape of a quantum dot ensemble that reflects its size distribution and are largely insensitive to its microscopic dynamics. Second, single quantum dot spectroscopy studies that circumvent inhomogeneous broadening have inherent limitations such as time resolution and dot-to-dot structural variations. These limitations have restricted the focus of most experimental studies to properties of discrete vibrational modes because the signatures of continuum-mode coupling are generally weak. Studies that do observe continuum modes are heavily influenced by spectral diffusion on time scales shorter than the integration time[28] and vary greatly between dots.[29]

A technique capable of extracting the homogeneous response of an inhomogeneously broadened ensemble is multidimensional coherent spectroscopy (MDCS),[30] which correlates absorption, intraband (Raman) coherence,[31] and emission spectra. MDCS has recently been applied to a variety of quantum dot systems, including interfacial,[32,33] self-assembled,[34,35] and colloidal[36−42] dots, to reveal physics normally obscured by inhomogeneous broadening or single-dot experiment limitations. MDCS provides material properties that are both ensemble-averaged and size-resolved for all resonance frequencies within the excitation bandwidth.

In this Letter, we use MDCS to study an ensemble of core/shell colloidal quantum dots (CQDs) at cryogenic temperatures. The third-order response that we measure via MDCS enhances vibrational lineshapes due to phonon coupling, allowing for a sensitive, direct characterization of acoustic phonon coupling in the material. We not only characterize

Received: August 23, 2019
Accepted: September 26, 2019
Published: September 26, 2019

DOI: 10.1021/acs.jpclett.9b02474
J. Phys. Chem. Lett. 2019, 10, 6144−6150

coupling to discrete acoustic modes related to the dot geometry[23] but also observe strong features characteristic of coupling to a continuum harmonic bath. We attribute this bath to continuum acoustic modes of the quantum dot lattice[43,44] and argue for the coexistence of both a bulk-like continuum and discrete torsional vibrations. By comparison to the simulation, we characterize the continuum-mode spectral density and coupling mechanism.

The sample is CQDs composed of a 2 nm mean radius CdSe core and a 2.5 nm mean thickness CdZnS shell (shown in Figure 1a), whose synthesis is detailed elsewhere.[45] To study their properties at cryogenic temperatures, we dispersed the CQDs in heptamethylnonane, which forms a transparent glass at temperatures <100 K and is liquid up to room temperature. The colloidal suspension is diluted to an optical density of 0.3 at the room-temperature 1S exciton absorption peak.

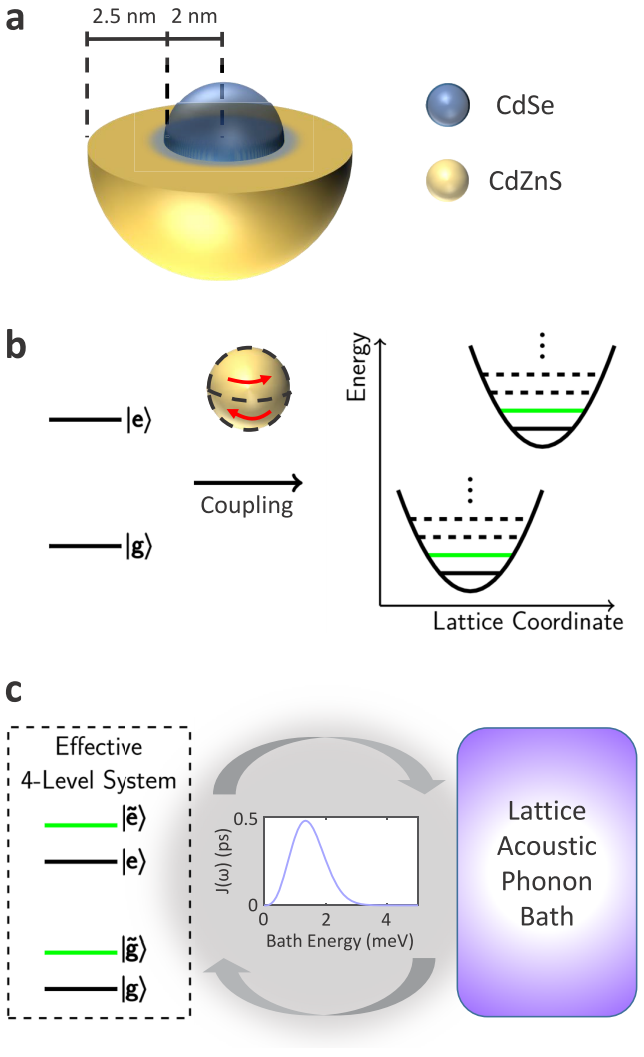

Figure 1. (a) Schematic of the CdSe/CdZnS core/shell colloidal quantum dots. (b) Dressing of the ground and excited exciton states by the $(l, n) = (2,0)$ torsional mode results in ladders of states separated by the (2,0) mode energy. (c) Simplified four-level system formed from the lowest two states of the ground- and excited-state ladders then couples to a harmonic bath of acoustic phonon continuum states. The coupling strength is characterized by the spectral density function $J(\omega)$, and the $J(\omega)$ used in the simulations below is plotted in the inset.

The finite size of the CQD geometry introduces discrete vibrations.[22,23] These vibrations may be separated into the two classes of acoustic and torsional modes, which have longitudinal and transverse character, respectively. However, acoustic modes of CQDs embedded in a matrix crucially depend on the difference in longitudinal sound velocities of the CQD and the matrix. For a large sound velocity mismatch, confined acoustic modes are sustained by reflections at the CQD surface.[27] However, a small sound velocity mismatch[43] gives rise to an acoustic continuum characteristic of delocalized vibrations in bulk materials[44] because boundary conditions at the CQD surface may be modified such that vibrations of the combined matrix and embedded sphere must be jointly considered.

MDCS is ideal to investigate acoustic phonon coupling in CQDs for two main reasons. First, the ensemble-averaged homogeneous response may be retrieved in the presence of inhomogeneity as a function of resonance energy (corresponding to the radius in CQDs). Second, vibrational lineshapes are enhanced by nonlinear spectroscopies such as MDCS.

An MDCS spectrum is generated by Fourier transforming a four-wave mixing signal along a combination of the two delays, τ and T, between three excitation pulses and the evolution time, t, after the last pulse. We acquire single-quantum spectra[42,46] by Fourier transforming along τ and t,[47] which correlates absorption and emission spectra of the sample. Rephasing single-quantum spectra circumvent inhomogeneity by rephasing the evolution of excited coherences (due to a phase-conjugated first pulse[46]), as reflected in the negative absorption energies, $\hbar\omega_\tau$. Cross-diagonal slices (taken perpendicular to the diagonal line $|\hbar\omega_\tau| = |\hbar\omega_t|$) provide the homogeneous third-order response.

To perform MDCS, we use a multidimensional optical nonlinear spectrometer (MONSTR).[47] 90 fs pulses at a 250 kHz repetition rate are split into four identical copies that are independently delayed in time and arranged in the box geometry. An excitation intensity of 4 W/cm^2 generates a predominately third-order response, as verified by the power dependence of the heterodyned signal, and causes negligible heating of the sample. (See the Supporting Information.) All pulses are colinearly polarized and centered at wavelength 605 nm. The laser spectrum is compared with the sample absorption spectrum in the Supporting Information.

Absolute-value single-quantum spectra are shown in the top row of Figure 2 and have three main features. First, a narrow zero-phonon line is present along the diagonal, which corresponds to absorption and emission at the same energy. Second, a prominent broad pedestal around the zero-phonon line,[48,49] which has the characteristic lineshape of localized excitons coupling to an acoustic phonon continuum bath,[50,51] grows with increasing temperature. At these low temperatures, the pedestal is asymmetric due to the higher probability of emission than the absorption of vibrational energy. Third, the acoustic phonon pedestal features two peaks next to the zero-phonon line (seen more clearly in Figure 3). Although the zero-frequency cutoff of the spectral density may result in a sharp feature on the Stokes side ($\hbar\omega_t - \hbar\omega_\tau < 0$) of the zero-phonon line, we cannot explain the anti-Stokes ($\hbar\omega_t - \hbar\omega_\tau > 0$) peak (marked by red arrows in Figure 3) through solely an acoustic phonon continuum. (See the Supporting Information.)

We explain these results by proposing that discrete torsional modes related to the quantum dot geometry exist in

DOI: 10.1021/acs.jpclett.9b02474
J. Phys. Chem. Lett. 2019, 10, 6144−6150

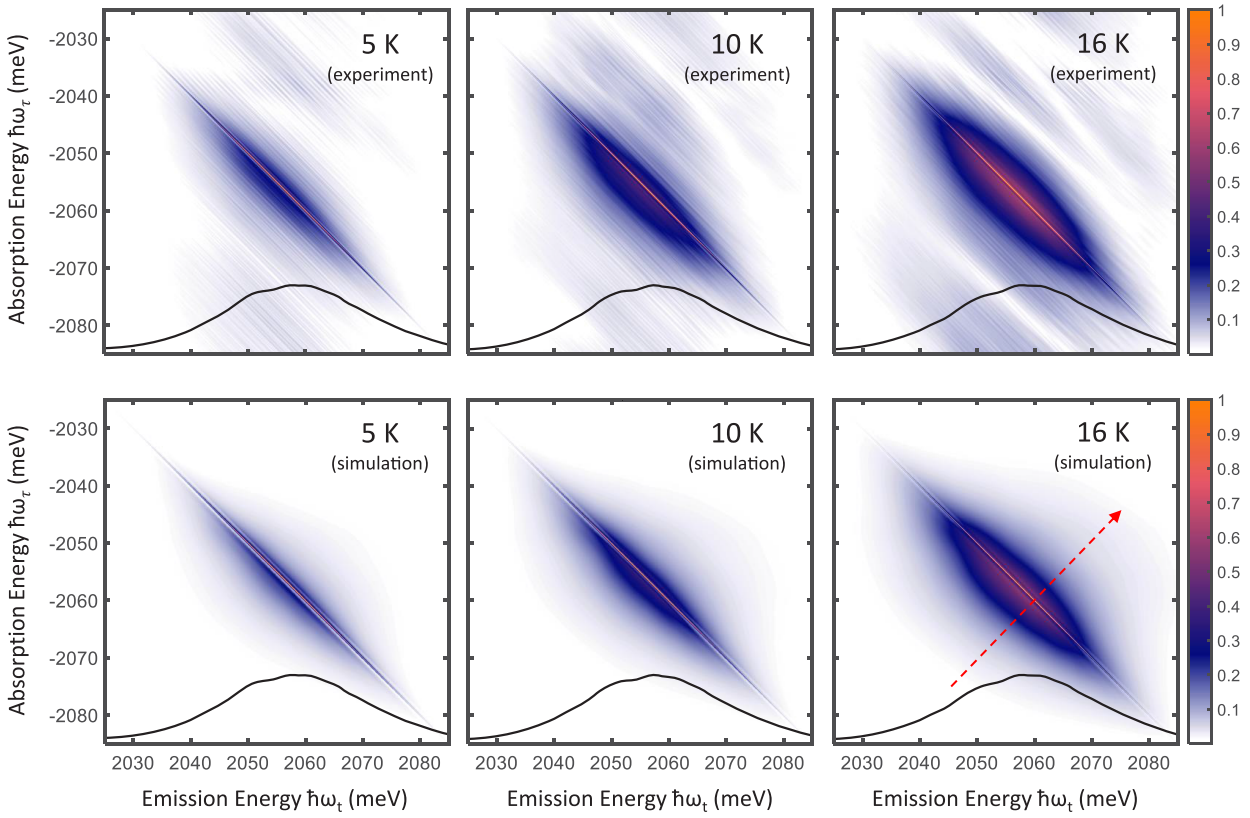

Figure 2. Experimental (top row) and simulated (bottom row) absolute-value single-quantum spectra at temperatures 5, 10, and 16 K. All spectra are taken at waiting time T = 1 ps. The solid black curves represent the spectra of the excitation and local oscillator pulses for each temperature. A red dashed arrow in the bottom right panel indicates the location of the slices shown in Figure 3.

conjunction with continuum longitudinal acoustic modes related to the crystal lattice. We were unable to find values for the low-temperature (glass phase) sound velocity for heptamethylnonane, although from its room-temperature (liquid-phase) speed,[52] 1.285 × 10^5 cm/s, it is plausible that in the solid form its longitudinal sound velocity may increase three to four times and become comparable to the CQD longitudinal sound velocity. (See the Supporting Information.) In this case, longitudinal vibrations may propagate into the surrounding glass matrix with minimal reflection at the dot boundary, giving rise to a continuum of longitudinal acoustic phonon modes. Simultaneously, transverse torsional modes involving no radial displacement into the surrounding matrix are supported by the dot geometry.

To investigate the validity of this interpretation, we simulate the acquired single-quantum spectra according to the following model. A discrete transverse torsional mode "dresses" the ground and excited electronic states to generate ladders of states separated by the torsional mode energy[53] (shown in Figure 1b). By calculating the allowed torsional mode energies (indexed by l and n) according to our material parameters, we find that the $(l, n) = (2,0)$ mode matches the features of our experimental spectra. (See the Supporting Information.) The comparison with spectra taken of smaller quantum dots also reveals larger torsional mode energies, which is consistent with this model. (See the Supporting Information.) We note that the higher frequency $(l, n) = (1,0)$ mode, which involves oscillations of a core and shell layer in opposite directions, should couple weakly to excitons in the type-I CdSe/CdZnS quantum dots studied here that confine both carriers in the CdSe core.[45] The transition strengths between these states are determined by the Huang−Rhys parameter, S.[54] The energies of these states are then modulated by a continuum bath of longitudinal acoustic phonons via elastic interactions. Assuming that the bath is harmonic, that is, the coupling is taken to be linear coupling to a continuous distribution of harmonic oscillators, we can characterize the system-bath interaction by a spectral density function, $J(\omega)$ (shown in Figure 1c). The spectral density may be loosely interpreted as the frequency spectrum of the energy gap modulation by a coupled harmonic bath. For a spherical quantum dot with identical electron and hole localization radii (which is the case for type-I CQDs in the strong confinement regime[55]), the spectral density of an acoustic phonon bath

$$J_a(\omega) = A\omega^p e^{-\omega^2/\omega_c^2} \quad (1)$$

may be derived analytically,[56] where A characterizes the coupling strength, ω_c is a cutoff frequency that determines the width of the acoustic phonon spectral features, and p is an integer that depends on the coupling mechanism (p = (1)3 for (deformation potential) piezoelectric coupling).[57] In single-quantum spectra, A, ω_c, and p determine the relative amplitude, width, and steepness of the central pedestal feature, respectively, and serve as orthogonal parameters that uniquely determine the size and shape of the pedestal. The experimental and simulated single-quantum spectra at temperatures 5, 10, and 16 K are shown in Figure 2. Corresponding simulations without torsional mode coupling, which fail to reproduce the anti-Stokes peak, may be found in the Supporting Information.

DOI: 10.1021/acs.jpclett.9b02474
J. Phys. Chem. Lett. 2019, 10, 6144−6150

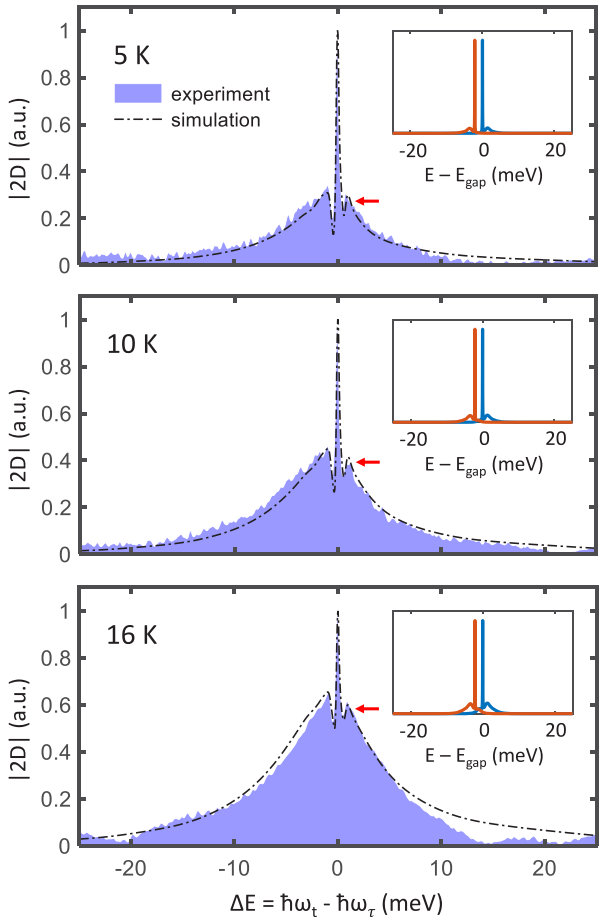

Figure 3. Cross-diagonal slices of the experimental (solid purple curve) and simulated (black line) absolute-value single-quantum spectra at temperatures 5, 10, and 16 K. The slice locations are indicated by the red dashed arrow in Figure 2. The corresponding simulated absorption (blue) and fluorescence (orange) lineshapes are plotted in the inset as a function of detuning from the thermally averaged ground-state electronic energy gap, E_{gap}.

For the model described above, analytic expressions are not available to fit experimental lineshapes. We thus emphasize that the goal of our simulations is not to extract numerical values for specific quantities but rather to elucidate the nature of the underlying microscopic dynamics. The torsional mode energy, $E_{(2,0)}$, is calculated,[22] while accounting for the core–shell structure of our dots (see the Supporting Information), to be 0.8 meV and is the value used in our simulation. The torsional mode Huang–Rhys parameter used is $S = 0.6$. We were unable to obtain a good agreement between the experiment and the simulation for the deformation potential coupling ($p = 1$) with the continuum acoustic modes. Although excitons in free-standing few-nanometer radii CQDs are thought to couple to acoustic vibrations predominately via the deformation potential mechanism,[22] our spectra suggest that the delocalized acoustic vibrations considered here couple through the long-range piezoelectric interaction ($p = 3$) used in our simulation. Coherences between states $|g\rangle$ and $|e\rangle$ are simulated with a dephasing rate $\hbar\gamma = 0.4$ meV to match the zero-phonon line width, whereas coherences involving the vibrationally excited states $|\tilde{g}\rangle$ and $|\tilde{e}\rangle$ dephase more quickly at $\hbar\gamma = 1.6$ meV. The remaining parameters used for the spectral density are $A = 0.47$ ps^4 and $\hbar\omega_c = 1.15$ meV. It should be noted that the simulated spectra in Figure 2 are obtained after numerically including finite pulse bandwidth effects (see the Supporting Information) for a large inhomogeneously broadened ($\sigma = 50$ meV) response function by using the respective experimental laser spectrum at each temperature.

In Figure 3, we plot cross-diagonal slices centered at energy $|\hbar\omega_\tau| = |\hbar\omega_t| = 2060$ meV. The comparison of the single-quantum spectrum slices with the simulated absorption and fluorescence lineshapes plotted in the inset contrasts the difference in strength (relative to the zero-phonon line) between the linear the and third-order vibrational lineshapes. The enhancement of vibrational lineshapes in the third-order response is due to additional terms involving the dephasing lineshape function that are absent in the linear response. (See the Supporting Information.) The nonlinear response of a system may therefore reveal vibrational couplings that are otherwise too weak to observe via linear spectroscopies.

In higher dimensional semiconductor nanostructures, many-body effects have been found to manifest in multidimensional spectra.[58,59] It is therefore important to characterize their role in our measurements. First, the effects of Coulomb correlation that gives rise to the excitonic states probed in our experiment are primarily characterized by a correlation energy that changes the energy gap[60] and do not modify the spectral density functional form[57] given by eq 1. In terms of higher order correlation effects, we neglect in our simulations excited-state absorption (ESA) pathways that involve doubly excited states with a binding energy of Δ_{XX}. Previous studies have determined Δ_{XX} to be tens of millielectronvolts[41,61] and beyond our laser bandwidth, so we do not expect these pathways to contribute to our single-quantum spectra. Our experimental parameters also correspond to fewer than 0.2 excitons per quantum dot (see the Supporting Information), which precludes significant nonlinear signals arising from excited initial states. Nevertheless, we verify this assumption by examining the quadratures of the complex spectrum at 16 K plotted in Figure 4a. Although the overall phase was not retrieved in our experiment, the complex single-quantum spectrum is phased in Figure 4 by maximizing the absorptive real part. We observe no evidence of ESA pathways, which would appear as an opposite sign sideband located at $\hbar\omega_t = |\hbar\omega_\tau| - \Delta_{XX}$ in the lower left region of the single-quantum spectra.[59] The corresponding quadratures of the simulated single-quantum spectrum are plotted in Figure 4b, which agree well with the experiment. To examine the quadratures more closely, slices of the experimental and simulated spectra are taken at the same positions as in Figures 2 and 3 and are plotted in Figure 4c. As shown by the experimental and simulated phases plotted in the inset, no phase flip (indicative of an ESA sideband) is observed in the pedestal region.

In conclusion, we have observed vibrational lineshapes in the third-order nonlinear response of a core–shell CQD ensemble that indicate the simultaneous existence of discrete and continuum acoustic vibrational modes. As a primary mechanism of energy loss and dephasing, understanding acoustic phonon coupling is crucial to the design and implementation of CQDs in optoelectronic devices. In particular, devices based on CQD-doped glasses[62] or superlattices,[63] and even other colloidal materials such as nanorods[64] or nanoplatelets,[65] should be designed with an engineered spectral density (via methods such as impurity doping[66,67] or varying the embedding layer) to minimize the

DOI: 10.1021/acs.jpclett.9b02474
J. Phys. Chem. Lett. 2019, 10, 6144–6150

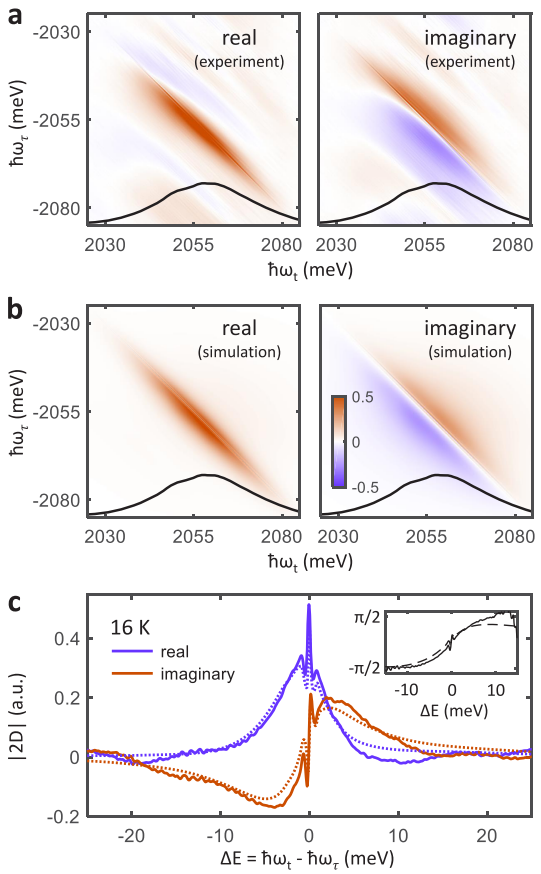

Figure 4. (a) Experimental and (b) simulated single-quantum spectrum quadratures at 16 K. The experimental spectrum is phased by maximizing the real-quadrature zero-phonon line. (c) Cross-diagonal slices of the experimental (solid lines) and simulated (dotted lines) single-quantum spectrum quadratures at 16 K. The inset shows the corresponding phase across the slice. The slice location is the same as indicated by the red dashed arrow in Figure 2.

energy loss and other dissipative processes due to interactions with acoustic vibrations.

■ ASSOCIATED CONTENT

Supporting Information

The Supporting Information is available free of charge on the ACS Publications website at DOI: 10.1021/acs.jpclett.9b02474.

Experimental details, an extended description of the model and simulation method, dot-size dependence of the torsional mode, and power-dependent effects (PDF)

■ AUTHOR INFORMATION

Corresponding Author

*E-mail: cundiff@umich.edu.

ORCID

Wan-Ki Bae: 0000-0002-3832-2449

Lazaro A. Padilha: 0000-0002-8825-6611

Steven T. Cundiff: 0000-0002-7119-5197

Notes

The authors declare no competing financial interest.

■ ACKNOWLEDGMENTS

This work was supported by the Department of Energy grant number DE-SC0015782. D.B.A. acknowledges support by a fellowship from the Brazilian National Council for Scientific and Technological Development (CNPq). L.A.P. acknowledges support from the FAPESP (project numbers 2013/16911-2 and 2016/50011-7).

■ REFERENCES

(1) Yuan, Z.; Kardynal, B. E.; Stevenson, R. M.; Shields, A. J.; Lobo, C. J.; Cooper, K.; Beattie, N. S.; Ritchie, D. A.; Pepper, M. Electrically Driven Single-Photon Source. *Science* **2002**, *295*, 102.

(2) Senellart, P.; Solomon, G.; White, A. High-Performance Semiconductor Quantum-Dot Single-Photon Sources. *Nat. Nanotechnol.* **2017**, *12*, 1026.

(3) Loss, D.; DiVincenzo, D. P. Quantum Computation with Quantum Dots. *Phys. Rev. A: At., Mol., Opt. Phys.* **1998**, *57*, 120−126.

(4) Kloeffel, C.; Loss, D. Prospects for Spin-Based Quantum Computing in Quantum Dots. *Annu. Rev. Condens. Matter Phys.* **2013**, *4*, 51−81.

(5) Gazzano, O.; Solomon, G. S. Toward Optical Quantum Information Processing with Quantum Dots Coupled to Microstructures. *J. Opt. Soc. Am. B* **2016**, *33*, C160−C175.

(6) Carey, G. H.; Abdelhady, A. L.; Ning, Z.; Thon, S. M.; Bakr, O. M.; Sargent, E. H. Colloidal Quantum Dot Solar Cells. *Chem. Rev.* **2015**, *115*, 12732−12763.

(7) Zhao, H.; Rosei, F. Colloidal Quantum Dots for Solar Technologies. *Chem.* **2017**, *3*, 229−258.

(8) Vasilevskiy, M. I. Exciton-Phonon Interaction in Semiconductor Nanocrystals. In *Semiconductor Nanocrystal Quantum Dots: Synthesis, Assembly, Spectroscopy and Applications*; Rogach, A. L., Ed.; Springer: Vienna, 2008; pp 217−255.

(9) Liu, A.; Bonato, L. G.; Sessa, F.; Almeida, D. B.; Isele, E.; Nagamine, G.; Zagonel, L. F.; Nogueira, A. F.; Padilha, L. A.; Cundiff, S. T. Three-Oscillator Vibrational Band-Gap Renormalization and Band-Tailing in $CsPbI_3$ Perovskite Nanocrystals. **2019**, arXiv:1908.04881. arXiv.org e-Print archive. https://arxiv.org/abs/1908.04881. (Accessed 9/28/19)

(10) Quilter, J. H.; Brash, A. J.; Liu, F.; Glässl, M.; Barth, A. M.; Axt, V. M.; Ramsay, A. J.; Skolnick, M. S.; Fox, A. M. Phonon-Assisted Population Inversion of a Single InGaAs/GaAs Quantum Dot by Pulsed Laser Excitation. *Phys. Rev. Lett.* **2015**, *114*, 137401.

(11) Kaldewey, T.; Lüker, S.; Kuhlmann, A. V.; Valentin, S. R.; Ludwig, A.; Wieck, A. D.; Reiter, D. E.; Kuhn, T.; Warburton, R. J. Coherent and Robust High-Fidelity Generation of a Biexciton in a Quantum Dot by Rapid Adiabatic Passage. *Phys. Rev. B: Condens. Matter Mater. Phys.* **2017**, *95*, 161302.

(12) Reindl, M.; Jöns, K. D.; Huber, D.; Schimpf, C.; Huo, Y.; Zwiller, V.; Rastelli, A.; Trotta, R. Phonon-Assisted Two-Photon Interference from Remote Quantum Emitters. *Nano Lett.* **2017**, *17*, 4090−4095.

(13) Poem, E.; Kodriano, Y.; Tradonsky, C.; Lindner, N. H.; Gerardot, B. D.; Petroff, P. M.; Gershoni, D. Accessing the Dark Exciton with Light. *Nat. Phys.* **2010**, *6*, 993.

(14) Masia, F.; Accanto, N.; Langbein, W.; Borri, P. Spin-Flip Limited Exciton Dephasing in CdSe/ZnS Colloidal Quantum Dots. *Phys. Rev. Lett.* **2012**, *108*, 087401.

(15) Lüker, S.; Kuhn, T.; Reiter, D. E. Phonon-Assisted Dark Exciton Preparation in a Quantum Dot. *Phys. Rev. B: Condens. Matter Mater. Phys.* **2017**, *95*, 195305.

(16) Gindele, F.; Hild, K.; Langbein, W.; Woggon, U. Temperature-Dependent Line Widths of Single Excitons and Biexcitons. *J. Lumin.* **2000**, *87*−*89*, 381−383.

(17) Valerini, D.; Cretí, A.; Lomascolo, M.; Manna, L.; Cingolani, R.; Anni, M. Temperature Dependence of the Photoluminescence Properties of Colloidal CdSeZnS Core/Shell Quantum Dots Embedded in a Polystyrene Matrix. *Phys. Rev. B: Condens. Matter Mater. Phys.* **2005**, *71*, 235409.

DOI: 10.1021/acs.jpclett.9b02474
J. Phys. Chem. Lett. 2019, 10, 6144−6150

(18) Liptay, T. J.; Marshall, L. F.; Rao, P. S.; Ram, R. J.; Bawendi, M. G. Anomalous Stokes Shift in CdSe Nanocrystals. *Phys. Rev. B: Condens. Matter Mater. Phys.* **2007**, *76*, 155314.
(19) Muljarov, E. A.; Zimmermann, R. Dephasing in Quantum Dots: Quadratic Coupling to Acoustic Phonons. *Phys. Rev. Lett.* **2004**, *93*, 237401.
(20) Accanto, N.; Masia, F.; Moreels, I.; Hens, Z.; Langbein, W.; Borri, P. Engineering the Spin-Flip Limited Exciton Dephasing in Colloidal CdSe/CdS Quantum Dots. *ACS Nano* **2012**, *6*, 5227−5233.
(21) Jakubczyk, T.; Delmonte, V.; Fischbach, S.; Wigger, D.; Reiter, D. E.; Mermillod, Q.; Schnauber, P.; Kaganskiy, A.; Schulze, J.-H.; Strittmatter, A.; et al. Impact of Phonons on Dephasing of Individual Excitons in Deterministic Quantum Dot Microlenses. *ACS Photonics* **2016**, *3*, 2461−2466.
(22) Takagahara, T. Electron-Phonon Interactions and Excitonic Dephasing in Semiconductor Nanocrystals. *Phys. Rev. Lett.* **1993**, *71*, 3577−3580.
(23) Kuok, M. H.; Lim, H. S.; Ng, S. C.; Liu, N. N.; Wang, Z. K. Brillouin Study of the Quantization of Acoustic Modes in Nanospheres. *Phys. Rev. Lett.* **2003**, *90*, 255502.
(24) Chilla, G.; Kipp, T.; Menke, T.; Heitmann, D.; Nikolic, M.; Frömsdorf, A.; Kornowski, A.; Förster, S.; Weller, H. Direct Observation of Confined Acoustic Phonons in the Photoluminescence Spectra of a Single CdSe-CdS-ZnS Core-Shell-Shell Nanocrystal. *Phys. Rev. Lett.* **2008**, *100*, 057403.
(25) Oron, D.; Aharoni, A.; de Mello Donega, C.; van Rijssel, J.; Meijerink, A.; Banin, U. Universal Role of Discrete Acoustic Phonons in the Low-Temperature Optical Emission of Colloidal Quantum Dots. *Phys. Rev. Lett.* **2009**, *102*, 177402.
(26) Huxter, V. M.; Scholes, G. D. Acoustic Phonon Strain Induced Mixing of the Fine Structure Levels in Colloidal CdSe Quantum Dots Observed by a Polarization Grating Technique. *J. Chem. Phys.* **2010**, *132*, 104506.
(27) Werschler, F.; Hinz, C.; Froning, F.; Gumbsheimer, P.; Haase, J.; Negele, C.; de Roo, T.; Mecking, S.; Leitenstorfer, A.; Seletskiy, D. V. Coupling of Excitons and Discrete Acoustic Phonons in Vibrationally Isolated Quantum Emitters. *Nano Lett.* **2016**, *16*, 5861−5865.
(28) Empedocles, S. A.; Bawendi, M. G. Influence of Spectral Diffusion on the Line Shapes of Single CdSe Nanocrystallite Quantum Dots. *J. Phys. Chem. B* **1999**, *103*, 1826−1830.
(29) Fernée, M. J.; Littleton, B. N.; Cooper, S.; Rubinsztein-Dunlop, H.; Gómez, D. E.; Mulvaney, P. Acoustic Phonon Contributions to the Emission Spectrum of Single CdSe Nanocrystals. *J. Phys. Chem. C* **2008**, *112*, 1878−1884.
(30) Cundiff, S. T.; Mukamel, S. Optical Multidimensional Coherent Spectroscopy. *Phys. Today* **2013**, *66*, 44−49.
(31) Ferrio, K. B.; Steel, D. G. Raman Quantum Beats of Interacting Excitons. *Phys. Rev. Lett.* **1998**, *80*, 786−789.
(32) Kasprzak, J.; Patton, B.; Savona, V.; Langbein, W. Coherent Coupling Between Distant Excitons Revealed by Two-Dimensional Nonlinear Hyperspectral Imaging. *Nat. Photonics* **2011**, *5*, 57.
(33) Martin, E. W.; Cundiff, S. T. Inducing Coherent Quantum Dot Interactions. *Phys. Rev. B: Condens. Matter Mater. Phys.* **2018**, *97*, 081301.
(34) Kasprzak, J.; Portolan, S.; Rastelli, A.; Wang, L.; Plumhof, J. D.; Schmidt, O. G.; Langbein, W. Vectorial Nonlinear Coherent Response of a Strongly Confined Exciton-Biexciton System. *New J. Phys.* **2013**, *15*, 055006.
(35) Suzuki, T.; Singh, R.; Bayer, M.; Ludwig, A.; Wieck, A. D.; Cundiff, S. T. Coherent Control of the Exciton-Biexciton System in an InAs Self-Assembled Quantum Dot Ensemble. *Phys. Rev. Lett.* **2016**, *117*, 157402.
(36) Turner, D. B.; Hassan, Y.; Scholes, G. D. Exciton Superposition States in CdSe Nanocrystals Measured Using Broadband Two-Dimensional Electronic Spectroscopy. *Nano Lett.* **2012**, *12*, 880−886.
(37) Harel, E.; Rupich, S. M.; Schaller, R. D.; Talapin, D. V.; Engel, G. S. Measurement of Electronic Splitting in PbS Quantum Dots by Two-Dimensional Nonlinear Spectroscopy. *Phys. Rev. B: Condens. Matter Mater. Phys.* **2012**, *86*, 075412.
(38) Karki, K. J.; Widom, J. R.; Seibt, J.; Moody, I.; Lonergan, M. C.; Pullerits, T.; Marcus, A. H. Coherent Two-Dimensional Photocurrent Spectroscopy in a PbS Quantum Dot Photocell. *Nat. Commun.* **2014**, *5*, 5869.
(39) Gellen, T. A.; Lem, J.; Turner, D. B. Probing Homogeneous Line Broadening in CdSe Nanocrystals Using Multidimensional Electronic Spectroscopy. *Nano Lett.* **2017**, *17*, 2809−2815.
(40) Park, S. D.; Baranov, D.; Ryu, J.; Cho, B.; Halder, A.; Seifert, S.; Vajda, S.; Jonas, D. M. Bandgap Inhomogeneity of a PbSe Quantum Dot Ensemble from Two-Dimensional Spectroscopy and Comparison to Size Inhomogeneity from Electron Microscopy. *Nano Lett.* **2017**, *17*, 762−771.
(41) Seiler, H.; Palato, S.; Sonnichsen, C.; Baker, H.; Kambhampati, P. Seeing Multiexcitons through Sample Inhomogeneity: Band-Edge Biexciton Structure in CdSe Nanocrystals Revealed by Two-Dimensional Electronic Spectroscopy. *Nano Lett.* **2018**, *18*, 2999−3006.
(42) Liu, A.; Almeida, D. B.; Bae, W. K.; Padilha, L. A.; Cundiff, S. T. Non-Markovian Exciton-Phonon Interactions in Core-Shell Colloidal Quantum Dots at Femtosecond Timescales. *Phys. Rev. Lett.* **2019**, *123*, 057403.
(43) Sirenko, A. A.; Belitsky, V. I.; Ruf, T.; Cardona, M.; Ekimov, A. I.; Trallero-Giner, C. Spin-Flip and Acoustic-Phonon Raman Scattering in CdS Nanocrystals. *Phys. Rev. B: Condens. Matter Mater. Phys.* **1998**, *58*, 2077−2087.
(44) Murray, D. B.; Saviot, L. Phonons in an Inhomogeneous Continuum: Vibrations of an Embedded Nanoparticle. *Phys. Rev. B: Condens. Matter Mater. Phys.* **2004**, *69*, 094305.
(45) Lim, J.; Jeong, B. G.; Park, M.; Kim, J. K.; Pietryga, J. M.; Park, Y.-S.; Klimov, V. I.; Lee, C.; Lee, D. C.; Bae, W. K. Influence of Shell Thickness on the Performance of Light-Emitting Devices Based on CdSe/Zn1-XCdXS Core/Shell Heterostructured Quantum Dots. *Adv. Mater.* **2014**, *26*, 8034−8040.
(46) Hamm, P.; Zanni, M. *Concepts and Methods of 2D Infrared Spectroscopy*, 1st ed.; Cambridge University Press, 2011.
(47) Bristow, A. D.; Karaiskaj, D.; Dai, X.; Zhang, T.; Carlsson, C.; Hagen, K. R.; Jimenez, R.; Cundiff, S. T. A Versatile Ultrastable Platform for Optical Multidimensional Fourier-Transform Spectroscopy. *Rev. Sci. Instrum.* **2009**, *80*, 073108.
(48) Palinginis, P.; Wang, H. High-Resolution Spectral Hole Burning in CdSe/ZnS Core/Shell Nanocrystals. *Appl. Phys. Lett.* **2001**, *78*, 1541−1543.
(49) Palinginis, P.; Tavenner, S.; Lonergan, M.; Wang, H. Spectral Hole Burning and Zero Phonon Linewidth in Semiconductor Nanocrystals. *Phys. Rev. B: Condens. Matter Mater. Phys.* **2003**, *67*, 201307.
(50) Krummheuer, B.; Axt, V. M.; Kuhn, T. Theory of Pure Dephasing and the Resulting Absorption Line Shape in Semiconductor Quantum Dots. *Phys. Rev. B: Condens. Matter Mater. Phys.* **2002**, *65*, 195313.
(51) Besombes, L.; Kheng, K.; Marsal, L.; Mariette, H. Acoustic Phonon Broadening Mechanism in Single Quantum Dot Emission. *Phys. Rev. B: Condens. Matter Mater. Phys.* **2001**, *63*, 155307.
(52) Luning Prak, D. J.; Jones, M. H.; Cowart, J. S.; Trulove, P. C. Density, Viscosity, Speed of Sound, Bulk Modulus, Surface Tension, and Flash Point of Binary Mixtures of 2,2,4,6,6-Pentamethylheptane and 2,2,4,4,6,8,8-Heptamethylnonane at (293.15 to 373.15) K and 0.1 MPa and Comparisons with Alcohol-to-Jet Fuel. *J. Chem. Eng. Data* **2015**, *60*, 1157−1165.
(53) May, V.; Kühn, O. *Charge and Energy Transfer Dynamics in Molecular Systems*, 3rd ed.; Wiley-VCH, 2011.
(54) de Jong, M.; Seijo, L.; Meijerink, A.; Rabouw, F. T. Resolving the Ambiguity in the Relation Between Stokes Shift and Huang-Rhys Parameter. *Phys. Chem. Chem. Phys.* **2015**, *17*, 16959−16969.
(55) Sahin, M.; Nizamoglu, S.; Kavruk, A. E.; Demir, H. V. Self-Consistent Computation of Electronic and Optical Properties of a

DOI: 10.1021/acs.jpclett.9b02474
J. Phys. Chem. Lett. 2019, 10, 6144−6150

Single Exciton in a Spherical Quantum Dot via Matrix Diagonalization Method. *J. Appl. Phys.* **2009**, *106*, 043704.
(56) Lüker, S.; Kuhn, T.; Reiter, D. E. Phonon Impact on Optical Control Schemes of Quantum Dots: Role of Quantum Dot Geometry and Symmetry. *Phys. Rev. B: Condens. Matter Mater. Phys.* **2017**, *96*, 245306.
(57) Calarco, T.; Datta, A.; Fedichev, P.; Pazy, E.; Zoller, P. Spin-Based All-Optical Quantum Computation with Quantum Dots: Understanding and Suppressing Decoherence. *Phys. Rev. A: At., Mol., Opt. Phys.* **2003**, *68*, 012310.
(58) Li, X.; Zhang, T.; Borca, C. N.; Cundiff, S. T. Many-Body Interactions in Semiconductors Probed by Optical Two-Dimensional Fourier Transform Spectroscopy. *Phys. Rev. Lett.* **2006**, *96*, 057406.
(59) Hao, K.; Specht, J. F.; Nagler, P.; Xu, L.; Tran, K.; Singh, A.; Dass, C. K.; Schüller, C.; Korn, T.; Richter, M. Neutral and Charged Inter-Valley Biexcitons in Monolayer $MoSe_2$. *Nat. Commun.* **2017**, *8*, 15552.
(60) Tyrrell, E. J.; Tomic, S. Effect of Correlation and Dielectric Confinement on 1S1/2(e)nS3/2(h) Excitons in CdTe/CdSe and CdSe/CdTe Type-II Quantum Dots. *J. Phys. Chem. C* **2015**, *119*, 12720−12730.
(61) Salvador, M. R.; Sreekumari Nair, P.; Cho, M.; Scholes, G. D. Interaction Between Excitons Determines the Non-linear Response of Nanocrystals. *Chem. Phys.* **2008**, *350*, 56−68.
(62) Dong, G.; Wang, H.; Chen, G.; Pan, Q.; Qiu, J. Quantum Dot-Doped Glasses and Fibers: Fabrication and Optical Properties. *Front. Mater.* **2015**, *2*, 13.
(63) Kagan, C. R.; Lifshitz, E.; Sargent, E. H.; Talapin, D. V. Building Devices from Colloidal Quantum Dots. *Science* **2016**, *353*, aac5523.
(64) Hu, M.; Wang, X.; Hartland, G. V.; Mulvaney, P.; Juste, J. P.; Sader, J. E. Vibrational Response of Nanorods to Ultrafast Laser Induced Heating: Theoretical and Experimental Analysis. *J. Am. Chem. Soc.* **2003**, *125*, 14925−14933.
(65) Flatten, L. C.; Christodoulou, S.; Patel, R. K.; Buccheri, A.; Coles, D. M.; Reid, B. P. L.; Taylor, R. A.; Moreels, I.; Smith, J. M. Strong Exciton-Photon Coupling with Colloidal Nanoplatelets in an Open Microcavity. *Nano Lett.* **2016**, *16*, 7137−7141.
(66) Karlin, K. D., Ed. *Prog. Inorg. Chem.*; John Wiley & Sons, Ltd, 2005.
(67) Smirnov, A. M.; Golinskaya, A. D.; Kotin, P. A.; Dorofeev, S. G.; Palyulin, V. V.; Mantsevich, V. N.; Dneprovskii, V. S. Photoluminescence and Nonlinear Transmission of Cu-Doped CdSe Quantum Dots. *J. Lumin.* **2019**, *213*, 29−35.

DOI: 10.1021/acs.jpclett.9b02474
J. Phys. Chem. Lett. 2019, 10, 6144−6150